Dynamics of generalized Gaussian polymeric structures in random layered flows

Divya Katyal and Rama Kant*
Department of Chemistry, University of Delhi, Delhi 110007, India
(Received 26 July 2014; revised manuscript received 14 March 2015; published 30 April 2015)

We develop a formalism for the dynamics of a flexible branched polymer with arbitrary topology in the presence of random flows. This is achieved by employing the generalized Gaussian structure (GGS) approach and the Matheron–de Marsily model for the random layered flow. The expression for the average square displacement (ASD) of the center of mass of the GGS is obtained in such flow. The averaging is done over both the thermal noise and the external random flow. Although the formalism is valid for branched polymers with various complex topologies, we mainly focus here on the dynamics of the flexible star and dendrimer. We analyze the effect of the topology (the number and length of branches for stars and the number of generations for dendrimers) on the dynamics under the influence of external flow, which is characterized by their root-mean-square velocity, persistence flow length, and flow exponent α. Our analysis shows two anomalous power-law regimes, viz., subdiffusive (intermediate-time polymer stretching and flow-induced diffusion) and superdiffusive (long-time flow-induced diffusion). The influence of the topology of the GGS is unraveled in the intermediate-time regime, while the long-time regime is only weakly dependent on the topology of the polymer. With the decrease in the value of α, the magnitude of the ASD decreases, while the temporal exponent of the ASD increases in both the time regimes. Also there is an increase in both the magnitude of the ASD and the crossover time (from the subdiffusive to the superdiffusive regime) with an increase in the total mass of the polymeric structure.

DOI: 10.1103/PhysRevE.91.042602 PACS number(s): 36.20.−r, 83.80.Rs, 47.57.−s

I. INTRODUCTION

The conformational and dynamical behaviors of an isolated polymer in external flow fields have been subjects of considerable interest [1–7]. This is due to the specific interest in dynamical properties of biopolymers (e.g., DNA) [1,2], the unusual drag reduction phenomenon (which changes drastically the large-scale statistics of turbulent flows with the addition of a small amount of polymer) [8,9], and emerging technology of microfluidic and nanofluidic devices [10]. A great deal of research has been devoted to the understanding of the dynamics of a linear polymer in nonrandom flows [1–4,11–15] and random flows [16–21]. Starting with the pioneering studies of Chu and co-workers for nonrandom elongational flow of a single chain [1,2], further investigations have been performed for shear [3,4,11] and mixed flows [12]. Less experimental progress has been achieved in random flows due to the difficulty in creating a random flow in a microscopic-size volume. This issue was resolved by Groisman and Steinberg, who were the first to discuss the phenomenon of elastic turbulence [18,22,23]. Polymer dynamics and statistics in a random flow with a shear component have been studied experimentally [24] and numerically [25–27]. Experimental validation of the coil-stretch transition that is observed in the single polymer in random flows (as first predicted by Lumley [9]) was achieved by Gerashchenko *et al.* [19] and other works show aperiodic tumbling and stretching in the shear-preferred direction [24]. In a recent paper, the dynamics and conformations of a single fluorescently stained DNA molecule were studied in a random flow created by the same unlabeled molecules [28].

The simplified theoretical approaches concerning the polymer dynamics focused mainly on the elastic dumbbell model [20,21,25,27,29,30]. The dumbbell model is the reduced Rouse approach with a single spring connecting two beads, which accounts for only the slowest oscillation mode of the polymer. A theoretical understanding of the dynamics of a polymer molecule in random flow was first given by Lumley [9]. Balkovsky *et al.* [29] confirmed and extended Lumley's approach, while Chertkov [30] further improved this methodology with the inclusion of an anharmonic resistance contribution in incompressible turbulent flow of polymer solution. Using this approach, the dynamics of polymers is further investigated in elongational and random flow [20,21,31] and random flow with mean shear [25–27]. The major drawback of the dumbbell model is that it cannot be used for branched polymeric structures such as stars and dendrimers. It is well known that the branching has a great influence on the polymer dynamics [32–34]. So it offers the exciting possibility to explore the influence of flows on the dynamics of a polymer with complex topologies and vice versa.

The classical Rouse model [35,36] was originally formulated to study the dynamics of linear flexible polymeric chains. The extension of the Rouse model for an arbitrary branched polymer introduced the concept of Gaussian generalized structures (GGSs) [37–40]. A deep understanding of the various static and dynamic quantities of flexible polymeric networks has been attained by employing the GGS approach [32,41–51]. Also, considerable progress has been achieved in the understanding of the connection between the complex underlying geometries such as stars and polymers [41–43,52], dendrimers [41–43,53–56], dendrimers built from stars [44,45], various kinds of fractal polymer networks, viz., Sierpinski gaskets [46,47] and Vicsek fractals (regular hyperbranched polymers) [48,49], and random structures such as small-world networks [50,51], with dynamical properties under the influence of external forces. Here the various kinds of external forces applied consist of a constant step force where the external force pulls a single bead [32,41–43,46–50],

*rkant@chemistry.du.ac.in; http://people.du.ac.in/∼rkant/

an oscillating shear force that is used to find the dynamical shear modulus [32,41–43,46–49,53], an alternating electric field that is used to understand the dielectric response of polar molecules embedded in nonpolar solvents [48,51], a truncated step force [42], and random forces that include uncorrelated, long-range correlated, and diblock forces [38]. These types of forces are important in understanding the unfolding dynamics of various polymers. The unfolding (stretching) of a star and dendrimer with [41] and without [42] hydrodynamic interactions under the influence of a step force has been analyzed. It is shown here that the displacement of the bead on which the external force acts has a constant velocity at very short and long times, while at intermediate times the influence of the topology of the polymer on its dynamics is displayed. Chen and Cai [54,55] analyzed various time-dependent correlation functions and the intrinsic viscosity. They used an analytical procedure for diagonalization of the connectivity matrix of trifunctional dendrimers. Proceeding to a more complex structure, the dependence of the dynamics of the finite Sierpinski-type networks mainly on the spectral dimension has been investigated [46,47]. These types of fractal networks showed scaling behavior of the dynamical quantities in the intermediate-frequency range in the absence of hydrodynamic interactions (HIs) [46], whereas no scaling was observed in the presence of HIs [47]. Distinct from the dendrimers and Sierpinski-type lattices, Vicsek fractals obey scaling for both Rouse-type and Zimm-type models [48,49]. In addition to the work on the flexible polymers, there have been several attempts to understand the dynamics of semiflexible polymers in solutions within the framework of the optimized Rouse-Zimm approach [57], where stiffness is incorporated by restricting the directions and orientations of the respective bond vectors [58–61]. While the above-mentioned works investigated branched polymer dynamics in the absence of external flow, there have been few attempts to understand their structural and rheological properties under shear flow for stars [33,62] and dendrimers [34,63].

In the present paper we develop a general formalism to study the dynamics of the GGS with complex architecture in random layered flows. We use the Matheron–de Marsily (MdM) model [64] for random flow, which can mimic various flow conditions depending upon its flow parameters. Using this model, Oshanin and Blumen [16,17] investigated the dynamics of the Rouse (linear) polymer and showed that the average square displacement (ASD) of the center of mass of the chain exhibits an anomalous time dependence. The exponent that characterizes the growth of the ASD is dependent on the statistical properties of random flow. The main focus of our work here is on the dynamics of the flexible star and the dendrimer in random flow. The paper is structured as follows. In Sec. II we introduce the concept of the GGS model and the statistical properties of the MdM flow pattern and present the mathematical formalism of the problem, beginning with the basic Langevin equation of motion that governs the dynamical behavior under arbitrary external forces. We derive the analytical expression for the ASD of the center of mass of branched polymers under external flow in the long-time limit. In Sec. III we discuss our results for stars and dendrimers and show how the ASD depends on the underlying topology (number and length of branches for stars and the number of generations for dendrimers). We summarize our paper with conclusions in Sec. IV.

II. MATHEMATICAL APPROACH

In this section we develop a mathematical formalism for the dynamics of a GGS in random layered flow. A GGS can be represented as consisting of N spherical beads connected to each other by harmonic springs; this is an extension of the classical Rouse approach [36]. The configuration of a GGS is given by the set of position vectors $\{R_i\}$, where $R_i(t) \equiv (R_{xi}(t), R_{yi}(t), R_{zi}(t)) \equiv (X_i(t), Y_i(t), Z_i(t))$ is the position vector of the ith bead at time t. Its dynamics under the influence of external force fields in the absence of hydrodynamic interactions and excluded-volume effects is given by the Langevin equation [36]

$$\zeta \frac{\partial R_i(t)}{\partial t} = -\frac{\partial U(\{R_k\})}{\partial R_i} + f_i(t), \tag{1}$$

where ζ is the friction coefficient of a single bead and $f_i(t)$ is the thermal random force on the ith bead. The random thermal forces are centered Gaussian processes, hence their mean is zero, i.e., $\langle f(t)\rangle = 0$, and their correlation function follows the fluctuation-dissipation theorem $\langle f_{i\alpha}(t) f_{j\beta}(t')\rangle = 2k_B T \zeta \delta_{ij}\delta_{\alpha\beta}\delta(t-t')$. Here α and β denote the directions (x, y, or z), δ_{ij} and $\delta_{\alpha\beta}$ are Kronecker delta functions, $\delta(t-t')$ is the Dirac delta function, T is the temperature, and k_B is the Boltzmann constant. The explicit expression for the potential energy $U(\{R_k\})$ in Eq. (1) is given by

$$U(\{R_k\}) = \frac{K}{2}\sum_{\alpha,m,n} R_{m\alpha} A_{mn} R_{n\alpha} - \sum_{\alpha,n} F_{n\alpha} R_{n\alpha}. \tag{2}$$

From this equation we can see that the potential energy contains two terms, with the first term indicating the harmonic interactions between monomers directly bound to each other and the second term signifying the influence of each component of the external random force on the beads $F_{n\alpha}$. In the first sum on the right-hand side of Eq. (2), all bonds have been assumed to be equal, with the spring constant $K = 3k_BT/b^2$, where b is the mean distance between the beads; the m,n summation is over the bead, the α summation runs over the components x, y, and z, and the GGS is taken into account through an $N \times N$ matrix $\mathbf{A} = (A_{mn})$. The matrix $\mathbf{A}$ is the so-called adjacency or connectivity matrix [37,38,65,66] and is symmetric: Its diagonal elements A_{mm} equal the number of bonds emanating from the mth bead and its off-diagonal elements A_{mn} are either -1 if m and n are connected or 0 otherwise.

Random-walk arguments show that the entropy of a polymer is quadratic in R when the extended polymer is much smaller than the contour length L of the polymer, which leads to Hooke's law [29]. However, in more realistic models, Hooke's law is replaced by a force diverging as the size of the polymer approaches L, which helps in accounting for their finite extensibility by modifying the spring constant, viz., $K_{\text{eff}} = Kf(R)$. The function $f(R)$ (independent of the system temperature) specifies the elastic properties of the polymer and reflects the physical strength of the bonds between the beads that can be different in different polymers. For a finitely extensible nonlinear elastic model of polymers, $f(R)$

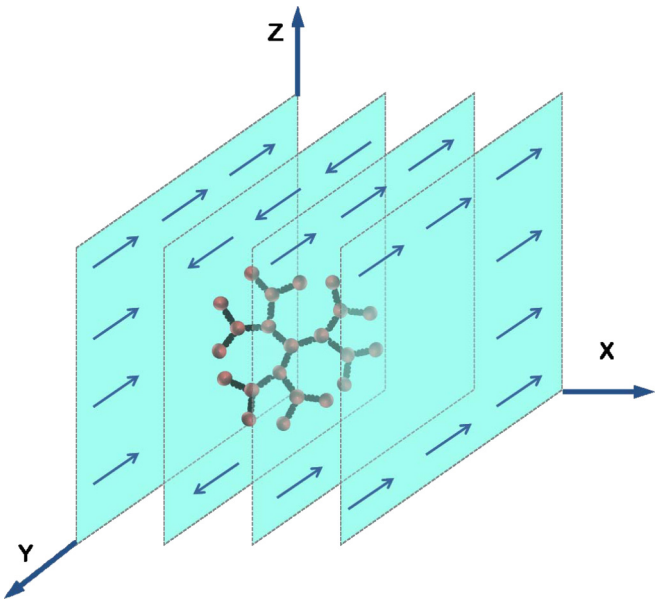

FIG. 1. (Color online) Schematic diagram of the GGS in the MdM flow pattern. The orientation of the velocity vector is a random function of the X variable and is constant within each layer.

is defined by the Warner law $f(R) = 1/(1 - R^2/L^2)$ and for a wormlike chain (which is useful in biological macromolecules) it is defined by the Marko-Siggia law $f(R) = 2/3 - L/6R + L/6R(1 - R/L)^2$ [7,31]. To avoid nonlinearity in this equation, one can replace R by its appropriate mean value [67].

Now inserting Eq. (2) into Eq. (1), we get a linearized Langevin equation describing the dynamics of the ith bead of the GGS in the external force

$$\zeta \frac{\partial R_i(t)}{\partial t} + K \sum_{j=1}^{N} A_{ij} R_j(t) = f_i(t) + \delta_{\alpha Y} F_i, \tag{3}$$

where F_i defines the force induced by the external random flow on the ith bead. To account for random flow we use the MdM model as shown in Fig. 1 (also see Refs. [16,17]). This type of model can be represented as a series of different layers parallel to each other and perpendicular to any axis, say, the X axis. While the orientation of the force vector is fixed within each layer, it varies randomly when going from one layer to the other. The random flow pattern produced by this particular model has similar randomness as in the random telegraph signal [68]. In general, the force or the velocity vector (as $V = F/\zeta$) is parallel to the Y axis and the X and Z components of the velocity vector are equal to zero. The Y component is taken to be a random function of the X coordinate

$$V_Y(X,Y,Z) = V[X]. \tag{4}$$

The random function $V[X]$ is assumed to be a Gaussian random function with the mean

$$\overline{V[X]} = 0 \tag{5}$$

and covariance

$$\overline{V[X_1]V[X_2]} = V_0^2 \phi(|X_1 - X_2|). \tag{6}$$

The overline represents the average over the random flow configurations, V_0 is the rms velocity of the flow, and the correlation function ϕ defines the correlation between various layers of the random flow. The random flow is assumed to be a stationary process, hence it is dependent only on the separation between the two layers. Another important transform of the quantity ϕ is the power spectrum $\mathcal{Q}(K)$, which is defined by the Fourier integral

$$\phi(|X_1 - X_2|) = \int_{-\infty}^{\infty} dK\, \mathcal{Q}(K) \exp[iK(X_1 - X_2)]. \tag{7}$$

We can model different types of flow behavior by choosing a specific form of the power spectrum $\mathcal{Q}(K)$. The dimension of $\mathcal{Q}(K)$ is length. An important case for the random layered flow field is that of the power-law power spectrum

$$\mathcal{Q}(K) = \frac{l_f}{2\pi} |l_f K|^{\alpha-1} = \frac{W|K^{\alpha-1}|}{2\pi V_0^2} \quad (0 < \alpha \leqslant 1), \tag{8}$$

where l_f is defined as the persistence length of flow. It is a measure of the distance between two layers of flow. Here α signifies the type of flow or, in other words, the persistence of the random flow. Its value lies between 0 and 1. Here $\alpha = 1$ indicates the δ-correlated flow. As the value of α decreases, the long-range correlation effects are enhanced, that is, they show a higher persistence of the flow. The prefactor W of the power-law power spectrum is a composite quantity that can be defined as

$$W = V_0^2 l_f^{\alpha}. \tag{9}$$

Therefore, the power-law power spectrum of random flow can mimic the different types of flow that are generated with a change in α, V_0, and l_f. The correlation function for the power-law spectrum in Eq. (8) can be obtained as

$$\phi(|X_1 - X_2|) = \frac{\Gamma(\alpha)\cos(\alpha\pi/2)}{\pi V_0^2} \frac{W}{|X_1 - X_2|^{\alpha}}, \tag{10}$$

where $\Gamma(\alpha)$ is the Gamma function. Equation (10) has a long-range algebraic distance-dependent correlation [17,69], while the simplest example of the power spectrum is the constant value that is the white-noise power spectrum, defined as

$$\mathcal{Q}(K) = \frac{l_f}{2\pi}. \tag{11}$$

When $\alpha \to 1$, Eq. (8) reduces to Eq. (11). This spectrum corresponds to the original MdM model with a δ-correlated flow field

$$\phi(|X_1 - X_2|) = l_f \delta(X_1 - X_2), \tag{12}$$

where δ is the Dirac delta function.

Usually the strength of flow in a polymeric system is characterized by the Weissenberg number Wi, which is the measure of relative intensity of elastic relaxation and stretching and is defined as the product of the longest relaxation time τ_P of the polymer and the characteristic velocity gradient V_0/l_f,

$$\mathrm{Wi} = \frac{V_0}{l_f} \tau_P. \tag{13}$$

To observe the influence of the polymeric structure on random flow, l_f must be much greater than the Kuhn segment length and can be of the order of the radius of gyration R_g of the polymeric structure. Since τ_P depends on the branching structure of the polymer, Wi will depend on the structure of the polymer of a given molecular weight.

A convenient and general way to find the solution of Eq. (3) is to write a matrix representation for different components of R_i, viz., X_i, Y_i, Z_i. At this stage it is important to emphasize that the simplicity in this problem arises due to the decoupling of the components of R_i. Therefore, the matrix representation of Eq. (3) for all components of the position vectors is given by

$$\frac{\partial \mathbf{X}(t)}{\partial t} + \sigma \mathbf{A}\mathbf{X}(t) = \frac{\mathbf{f}(t)}{\zeta}, \tag{14}$$

$$\frac{\partial \mathbf{Z}(t)}{\partial t} + \sigma \mathbf{A}\mathbf{Z}(t) = \frac{\mathbf{f}(t)}{\zeta}, \tag{15}$$

and

$$\frac{\partial \mathbf{Y}(t)}{\partial t} + \sigma \mathbf{A}\mathbf{Y}(t) = \frac{1}{\zeta}[\mathbf{f}(t) + \mathbf{F}(t)], \tag{16}$$

with $\sigma = K/\zeta$, $\mathbf{R} \equiv (R_1, R_2, \ldots, R_N)^T$, $\mathbf{f} \equiv (f_1, f_2, \ldots, f_N)^T$, and $\mathbf{F} \equiv (F_1, F_2, \ldots, F_N)^T$, where T denotes the transposed vector. The solution of Eqs. (14) and (15) represents the conventional diffusive motion (due to the random thermal force) of the beads in the X and Z directions, respectively. The solution of Eq. (16) represents the bead motion due to both the external flow and the thermal fluctuation (as the direction of the flow is in the Y direction). Equations (14)–(16) have the formal solutions

$$\mathbf{X}(t) = \frac{1}{\zeta}\int_{-\infty}^{t} dt' \exp[-\sigma(t-t')\mathbf{A}]\mathbf{f}(t'), \tag{17}$$

$$\mathbf{Z}(t) = \frac{1}{\zeta}\int_{-\infty}^{t} dt' \exp[-\sigma(t-t')\mathbf{A}]\mathbf{f}(t'), \tag{18}$$

$$\mathbf{Y}(t) = \frac{1}{\zeta}\int_{-\infty}^{t} dt' \exp[-\sigma(t-t')\mathbf{A}][\mathbf{f}(t') + \mathbf{F}(t')]. \tag{19}$$

Now, as we are interested in the ASD in the Y direction, we will use Eq. (19) as the basis for our further calculations.Equation (19) can be verified by differentiating the right-hand side with respect to t and it can also be rewritten as

$$\mathbf{Y}(t) - \exp[-\sigma t\mathbf{A}]\mathbf{Y}(0) = \frac{1}{\zeta}\int_{0}^{t} dt' \exp[-\sigma(t-t')\mathbf{A}][\mathbf{f}(t') + \mathbf{F}(t')], \tag{20}$$

by which the role of $Y(0)$ is rendered explicit. Thus, in Eq. (20) the solution starts at $t = 0$. An important quantity to understand in the dynamics of branched polymers under complex external flow is the displacement of the center of mass. The displacement of the center of mass, written in terms of the vector $\mathbf{u} \equiv (1, 1, \ldots, 1, \ldots, 1, 1)$, is defined as

$$\mathbf{R}_{\text{c.m.}}(t) = \frac{\sum_j \mathbf{R_j(t)}}{N} = \frac{\mathbf{u}\cdot\mathbf{R(t)}}{N}. \tag{21}$$

Simplifying Eq. (20) for the center of mass for the single component, say, the Yth component [assuming $X_{\text{c.m.}}(t=0) = 0$, $Y_{\text{c.m.}}(t=0) = 0$, and $Z_{\text{c.m.}}(t=0) = 0$], gives

$$\mathbf{Y}_{\text{c.m.}}(t) = \frac{1}{N\zeta}\int_{0}^{t} dt' \mathbf{u}\cdot\exp[-\sigma(t-t')\mathbf{A}][\mathbf{f}(t') + \mathbf{F}(t')] = \frac{1}{N\zeta}\int_{0}^{t} dt' \sum_{j=0}^{\infty} \mathbf{u}\cdot\frac{[-\sigma(\mathbf{t}-\mathbf{t}')\mathbf{A}]^{\mathbf{j}}}{\mathbf{j}!}[\mathbf{f}(\mathbf{t}') + \mathbf{F}(\mathbf{t}')]. \tag{22}$$

Since $\mathbf{u}\cdot\mathbf{A} = 0$ [either from $\det(A) = 0$ or by construction], in the sum over j only the term with $j = 0$ survives. Hence, Eq. (22) can be written as

$$Y_{\text{c.m.}}(t) = \frac{1}{N\zeta}\int_{0}^{t} dt' \mathbf{u}[\mathbf{f}(t') + \mathbf{F}(t')]. \tag{23}$$

The quantity of practical interest is $\overline{\langle Y^2_{\text{c.m.}}(t)\rangle}$, where the angular brackets represent the thermal averaging over various configurations of polymers and the overline represents the averaging over various configurations of random flow. For the sake of simplicity and avoiding the complexity of solving the expression for the ASD, the two averages are assumed to be independent of each other, i.e., our assumption implies that the nature of the thermal force is independent of the presence of the random external flow force (see Refs. [16,17]). To calculate $\overline{\langle Y^2_{\text{c.m.}}(t)\rangle}$ we first take the square of Eq. (23), which gives

$$Y^2_{\text{c.m.}}(t) = \frac{1}{N^2\zeta^2}\int_0^t dt' \int_0^t dt'' \sum_{m,n}[f_m(t')f_n(t'') + f_m(t')F_n(t'') + f_n(t'')F_m(t') + F_m(t')F_n(t'')]. \tag{24}$$

Using Eqs. (5) and (6) and averaging Eq. (24) over various configurations of random flow gives

$$\overline{Y^2_{\text{c.m.}}(t)} = \frac{1}{N^2\zeta^2}\int_0^t dt' \int_0^t dt'' \sum_{m,n}[f_m(t')f_n(t'')] + \frac{V_0^2}{N^2}\int_0^t dt' \int_0^t dt'' \sum_{m,n}\int_{-\infty}^{\infty} dK\, Q(K) e^{iK[X_m(t') - X_n(t'')]}. \tag{25}$$

Then, taking thermal average using fluctuation-dissipation theorem, we obtain

$$\overline{\langle Y^2_{\text{c.m.}}\rangle} = \frac{2k_BT}{N\zeta}t + \frac{V_0^2}{N^2}\int_0^t dt' \int_0^t dt'' \sum_{m,n}\int_{-\infty}^{\infty} dK\, Q(K)\langle e^{iK[X_m(t') - X_n(t'')]}\rangle. \tag{26}$$

We can define the quantity called the dynamic structure factor $g(K,t',t'')$ as

$$g(K,t',t'') = \frac{1}{N}\sum_{m,n}\langle e^{iK[X_m(t')-X_n(t'')]}\rangle. \tag{27}$$

The dynamic structure factor for $t' = 0$ gives

$$g(K,0,t'') = \frac{1}{N}\sum_{m,n}\langle e^{iK[X_m(0)-X_n(t'')]}\rangle. \tag{28}$$

For a Gaussian process, Eq. (28) is simplified using a cumulant expansion [36,68], where we use the fact that $\langle X_i(t')\rangle = 0$ for all i,

$$g(K,0,t'') = \frac{1}{N}\sum_{m,n} e^{-K^2\langle[X_m(0)-X_n(t'')]^2\rangle/2}. \tag{29}$$

Since the random process $X_m(t') - X_n(t'')$ is stationary in time and also due to the symmetry of the dynamic structure factor with respect to the time variables, the ASD of the center of mass can be written as

$$\overline{\langle Y^2_{\text{c.m.}}\rangle} = \frac{2k_BT}{N\zeta}t + \frac{2V_0^2}{N}\int_0^t dt'\int_0^{t'} dt''\int_{-\infty}^{\infty} dK\,\mathcal{Q}(K)g(K,t''). \tag{30}$$

The first term in Eq. (30) indicates the diffusion of the N-bead polymeric system due to the thermal fluctuations and it does not possess any structural information, while the second term depends upon the structure of the polymer through the dynamic structure function. The additional contribution to the ASD arises due to the weighted average from the power spectrum and the dynamic structure function.

In order to obtain a formal expression for the influence of the power spectrum of random flow on the ASD, we combine Eqs. (29) and (30). The ASD equation is

$$\overline{\langle Y^2_{\text{c.m.}}\rangle} = \frac{2k_BT}{N\zeta}t + \frac{2V_0^2}{N^2}\int_0^t dt'\int_0^{t'} dt''\sum_{m,n}\int_{-\infty}^{\infty} dK\,\mathcal{Q}(K)e^{-K^2\langle[X_m(0)-X_n(t'')]^2\rangle/2}. \tag{31}$$

The explicit expression for the ASD is obtained by substituting Eq. (8) for the power-law spectrum in Eq. (31) as

$$\overline{\langle Y^2_{\text{c.m.}}\rangle} = \frac{2k_BT}{N\zeta}t + \frac{W\Gamma(\alpha/2)}{\pi N^2}\sum_{m,n}\int_0^t dt'\int_0^{t'} dt''\langle[X_m(0)-X_n(t'')]^2\rangle^{-\alpha/2}, \tag{32}$$

where $W = V_0^2 l_f^{\alpha}$ and has dimensions of $(\text{length})^{2+\alpha}/(\text{time})^2$. For the white-noise spectrum ($\alpha = 1$) it simplifies as

$$\overline{\langle Y^2_{\text{c.m.}}\rangle} = \frac{2k_BT}{N\zeta}t + \frac{W}{N^2}\sum_{m,n}\int_0^t dt'\int_0^{t'} dt''\{\pi\langle[X_m(0)-X_n(t'')]^2\rangle\}^{-1/2}. \tag{33}$$

To find $\overline{\langle Y^2_{\text{c.m.}}(t)\rangle}$ one needs to know $\langle[X_m(t')-X_n(t'')]^2\rangle$, where $[X_m(t')-X_n(t'')]$ denotes the X component of the displacement of the mth bead at time t' with respect to the nth bead at time t'',

$$\langle[X_m(t')-X_n(t'')]^2\rangle = \langle[X_m(t')]^2\rangle + \langle[X_n(t'')]^2\rangle - 2\langle[X_m(t')X_n(t'')]\rangle. \tag{34}$$

In general, the covariance matrix for the X component is given by

$$\begin{aligned}\langle\mathbf{X}(t')\mathbf{X}^T(t'')\rangle &= \frac{1}{\zeta^2}\int_{-\infty}^{t'} dt_1\int_{-\infty}^{t''} dt_2 e^{-\sigma(t'-t_1)\mathbf{A}}\langle f(t_1)f^T(t_2)\rangle e^{-\sigma(t''-t_1)\mathbf{A}}\\ &= \frac{2k_BT}{\zeta}\int_{-\infty}^{t''} dt_2 e^{-\sigma(t'+t''-2t_2)\mathbf{A}}.\end{aligned} \tag{35}$$

In writing Eq. (35) we have used the fact that $f(\mathbf{A})^T = f(\mathbf{A})$. We now diagonalize $\mathbf{A}$ in the usual fashion by determining first N linearly independent normalized eigenvectors $\mathbf{Q_i}$ of $\mathbf{A}$, so that $\mathbf{A}\mathbf{Q}_i = \lambda_i\mathbf{Q}_i$. We set $\mathbf{Q} \equiv (\mathbf{Q}_1,\mathbf{Q}_2,\ldots,\mathbf{Q}_N)$ and have $\mathbf{AQ} = \mathbf{Q}\Lambda$, where Λ is the diagonal matrix whose elements are λ_i. Then

$$\mathbf{A} = \mathbf{Q}\Lambda\mathbf{Q^{-1}} \tag{36}$$

holds, with $\mathbf{Q^{-1}}$ being the inverse of $\mathbf{Q}$. From Eq. (36) any function of $\mathbf{A}$ can be written as

$$f(\mathbf{A}) = \mathbf{Q}f(\Lambda)\mathbf{Q^{-1}}. \tag{37}$$

In particular one has

$$\exp(\mathbf{A}t) = \mathbf{Q}\exp(\Lambda t)\mathbf{Q^{-1}}. \tag{38}$$

Thus, Eq. (35) can be written in terms of these eigenvalues and eigenvectors as

$$\langle \mathbf{X}(t')\mathbf{X}^T(t'')\rangle = \frac{2k_BT}{\zeta}\int_{-\infty}^{t''} dt_2 \mathbf{Q} e^{-\sigma(t'+t''-2t_2)\Lambda}\mathbf{Q}^{-1}. \tag{39}$$

We use the operator $\mathbf{u}_m \equiv (0,0,\ldots,1,\ldots,0,0)$ to project out the mth element in Eq. (39) to write the expression of Eq. (34) as

$$\begin{aligned}\langle [X_m(t') - X_n(t'')]^2\rangle &= \mathbf{u}_m\langle \mathbf{X}(t')\mathbf{X}^T(t')\rangle\mathbf{u}_m^T + \mathbf{u}_n\langle \mathbf{X}(t'')\mathbf{X}^T(t'')\rangle\mathbf{u}_n^T - 2\mathbf{u}_m\langle \mathbf{X}(t')\mathbf{X}^T(t'')\rangle\mathbf{u}_n^T \\ &= \frac{2k_BT}{\zeta}\sum_i\left[\int_{-\infty}^{t'} dt_2 Q_{mi}e^{-2\sigma(t'-t_2)\lambda_i}Q_{im}^{-1} + \int_{-\infty}^{t''} dt_2 Q_{ni}e^{-2\sigma(t''-t_2)\lambda_i}Q_{in}^{-1}\right. \\ &\quad \left. - 2\int_{-\infty}^{t''} dt_2 Q_{mi}e^{-\sigma(t'+t''-2t_2)\lambda_i}Q_{in}^{-1}\right].\end{aligned} \tag{40}$$

Isolating the $\lambda_1 = 0$ term in Eq. (40) and integrating it while taking into account that $Q_{m1} = Q_{1m}^{-1} = 1/\sqrt{N}$ for all values of m, we obtain

$$\langle [X_m(t') - X_n(t'')]^2\rangle = \frac{2k_BT}{N\zeta}|t'-t''| + \frac{k_BT}{\sigma\zeta}\sum_{i\neq 1}\left[Q_{mi}Q_{im}^{-1}/\lambda_i + Q_{ni}Q_{in}^{-1}/\lambda_i - 2Q_{mi}e^{-\sigma|t'-t''|\lambda_i}Q_{in}^{-1}/\lambda_i\right]. \tag{41}$$

The time integral in Eq. (32) cannot be solved exactly as the difference correlation function in Eq. (41) has a complicated form. Hence, one needs to expand the integrand for short- and long-time limits. For the short-time limit, i.e., at times much shorter than the Rouse relaxation time τ_R ($t'' \ll \tau_R$), the expansion will dominantly have information about individual segments or bead relaxation as it shows ballistic motion of individual beads. Also, the velocity vector stays more or less constant at short times, so it takes a time much longer than τ_R to encounter various layers along the X axis. Since, in this short-time regime, the dynamics does not possess any structural information about the polymer, we focus only on the long-time limit that gives all the information about the topology of the polymer and its interaction with the random flow. For the long-time limit, i.e., $t'' > \tau_R$, the final result for $\overline{\langle Y_{\text{c.m.}}^2\rangle}$ for the power-law spectrum (see the Appendix) is given by

$$\overline{\langle Y_{\text{c.m.}}^2\rangle} = \frac{2k_BT}{N\zeta}t + \frac{4W\Gamma(\alpha/2)}{\pi(4-\alpha)(2-\alpha)}\left(\frac{\zeta N}{2k_BT}\right)^{\alpha/2}t^{2-\alpha/2}\left\{1 - \mathcal{C}_1\left(\frac{\pi^2\tau_R}{2t}\right)^{1-\alpha/2} + \mathcal{C}_2\left(\frac{\pi^2\tau_R}{2t}\right) - \cdots\right\}, \tag{42}$$

where

$$\mathcal{C}_1 = \frac{4-\alpha}{2}\left(\frac{1}{N}\right)^{3-\alpha/2}\sum_{m,n}\left(\sum_{i\neq 1}C_i^{mn}\right)^{1-\alpha/2},$$

$$\mathcal{C}_2 = \frac{4-\alpha}{2N^3}\sum_{m,n}\left(\sum_{i\neq 1}C_i^{mn}\right),$$

$$C_i^{mn} = \frac{Q_{mi}Q_{im}^{-1}}{\lambda_i} + \frac{Q_{ni}Q_{in}^{-1}}{\lambda_i}.$$

The Rouse relaxation time in Eq. (42) is defined as $\tau_R = \zeta b^2N^2/3\pi^2k_BT$. The first term in Eq. (42) signifies the drift due to the thermal fluctuations, the prefactor of the second term represents the anomalous drift due to the external random flow, and the terms in curly brackets indicate the contributions from the stretch dynamics of the polymer. Since in the long-time limit the contribution due to the thermal fluctuations is negligibly small, the first term can be neglected. The special case for the linear polymer obtained numerically from Eq. (42) shows the same behavior as that given by the continuum model of Ref. [17].

Similarly, we can calculate the ASD for the δ-correlated flow. Also, by substituting $\alpha = 1$ in Eq. (42), we can directly obtain the result given as

$$\overline{\langle Y_{\text{c.m.}}^2\rangle} = \frac{2k_BT}{N\zeta}t + \frac{4W}{3}\left(\frac{\zeta N}{2\pi k_BT}\right)^{1/2} \times t^{3/2}\left\{1 - \mathcal{C}_1\left(\frac{\pi^2\tau_R}{2t}\right)^{1/2} + \mathcal{C}_2\left(\frac{\pi^2\tau_R}{2t}\right) - \cdots\right\}, \tag{43}$$

where

$$\mathcal{C}_1 = \frac{3}{2}\left(\frac{1}{N}\right)^{5/2}\sum_{m,n}\left(\sum_{i\neq 1}C_i^{mn}\right)^{1/2},$$

$$\mathcal{C}_2 = \frac{3}{2N^3}\sum_{m,n}\left(\sum_{i\neq 1}C_i^{mn}\right).$$

Therefore, in the long-time limit, Eqs. (42) and (43) give the final results for the ASD of the center of mass of the GGS in the case of flows with long-range correlation and δ-correlated flow, respectively.

III. DYNAMICS OF STARS AND DENDRIMERS

In this section we study the dynamics of regular star and regular dendrimer structures by using the expression for the ASD of the center of mass of the chain obtained in the previous

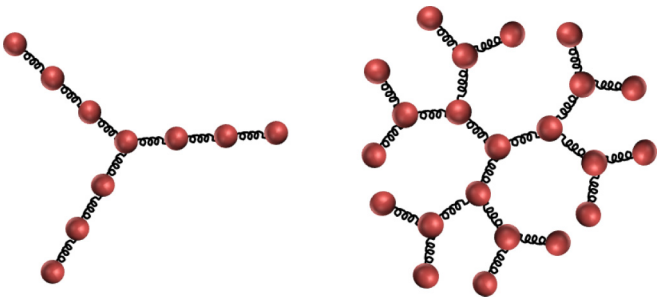

FIG. 2. (Color online) Schematic diagram of a star and a dendrimer. The parameters are $n = 3$ and $f = 3$ for the star and $G = 3$ and $f = 3$ for the dendrimer.

section [see Eqs. (42) and (43)]. In order to determine the ASD, both the eigenvalues λ_i and the eigenvectors Q_i of the adjacency matrix $\mathbf{A}$ are required, which we obtained by numerically diagonalizing the matrix $\mathbf{A}$. We used *Mathematica* software for the numerical calculations and for generating graphs. In the following two sections we will discuss the dynamics of stars and dendrimers, respectively.

A. Regular stars

Star polymers are structures comprised of polymer chains linked with one end to a common core. These structures have attracted much attention both in the field of theory [70,71] and in experiments [72,73]. Various experimental techniques are employed to characterize the structural properties of star polymers such as light scattering [74,75], small-angle neutron scattering [76,77], and x-ray-scattering techniques [78,79]. The basic feature of the star polymer is that it emerges from a central core bead, to which f arms are attached, each consisting of n beads. Hence the star polymer consists of a total number of beads $N = nf + 1$ and a total number of bonds $N - 1$ (see Fig. 2).

To generate our graphs we have assumed that each bead and spring is made up of N_0 Kuhn segments so that the effective friction coefficient $\zeta = N_0\zeta_0$ and the effective segment length (made up of N_0 segments) becomes $b = \sqrt{N_0}b_0$, where ζ_0 is the friction coefficient of each Kuhn segment and b_0 is the Kuhn segment length. Taking $N_0 \simeq 100$, the longest resultant relaxation times is on the order of 10 s, which is a typical experimental time scale for large realistic polymers [18,22,23]. The other parameters that we used are $\zeta_0 = 0.35 \times 10^{-6}$ dyn s/cm, $b_0 = 6.7 \times 10^{-8}$ cm, and $k_BT = 4.11 \times 10^{-14}$ erg at 298 K. The ASD in all figures is scaled with respect to the square of the radius of gyration of the linear chain $\langle R_g^2\rangle = Nb^2/6$.

In Fig. 3 we display the effect of star topology on its dynamics under the influence of an external random flow with $\alpha = 1$ and $W = 5 \times 10^{-13}$ cm^3/s^2. Using Eq. (43), the ASD of the center of mass $\overline{\langle Y^2_{\text{c.m.}}\rangle}^*$ is plotted against the time t^*, where in both cases the asterisk indicates that the quantities are given in dimensionless units, so $\overline{\langle Y^2_{\text{c.m.}}\rangle}^* = \overline{\langle Y^2_{\text{c.m.}}\rangle}/\langle R_g^2\rangle$ and $t^* = \sigma t$. Here the scaling of the ASD is done with $\langle R_g^2\rangle$ for a linear chain of 201 beads. The length of the arms is kept constant by taking $n = 100$ and varying the functionality f with $N = 201$, 301, 601, and 1201. We distinguish two different time regimes: intermediate- and long-time regimes. The intermediate-time

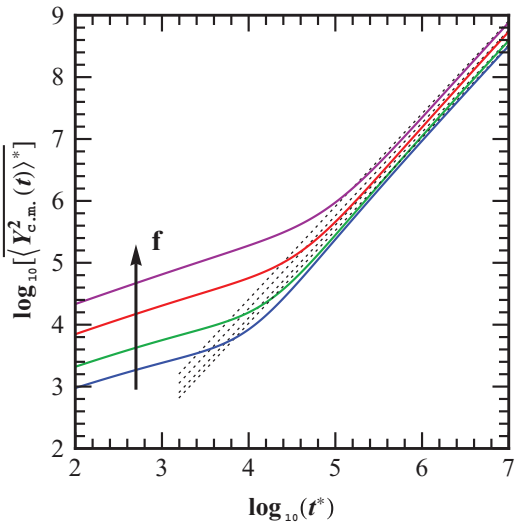

FIG. 3. (Color online) Dynamics of the center of mass of the star polymer under the influence of external random flow. Plotted on a logarithmic scale is the dimensionless ASD $\overline{\langle Y^2_{\text{c.m.}}\rangle}^* = \overline{\langle Y^2_{\text{c.m.}}\rangle}/\langle R_g^2\rangle$ vs dimensionless time $t^* = \sigma t$ for a fixed number of beads per arm $n = 100$ and a varying number of branches $f = 2$, 3, 6, and 12 with the total number of beads $N = 201$, 301, 601, and 1201, respectively (from bottom to top). Black dotted lines represents the drift term due to random external flow. The flow parameters are $\alpha = 1$ and $W = 5 \times 10^{-13}$ cm^3/s^2.

regime corresponds to the internal motion of the chain where $\overline{\langle Y^2_{\text{c.m.}}\rangle} \propto t^{\nu}$ with $\nu = 0.46 \pm 0.01 < 1$, i.e., it shows subdiffusive behavior. It is observed that the magnitude of the ASD is greater for the star with greater f, although the length of the arm is the same. On physical grounds, this is due to the fact that with increasing f, the total mass of the star grows, resulting in a greater stretching of the star as now there are more bonds that undergo stretching, which results in an increase in the ASD of the center of mass. The maximum stretching of the star polymer with $f = 12$ is about three times greater than that of the linear polymer ($f = 2$). Due to the external random flow there is an increase in the time dependence of the ASD in the long-time regime, where it exhibits superdiffusive behavior with $\nu = 1.54 \pm 0.01 > 1$, contributing to the overall diffusion of polymer. Again in this time regime, the magnitude of the ASD is greater for the star with greater f, i.e., the star with greater total mass moves faster than the star with lesser total mass, a result that is in agreement with the results of Refs. [16,17] for the Rouse chain.

In addition, we observe that as the total mass of the polymer increases, there is a delay in the crossover time t_c^* from intramolecular motion to overall polymer diffusion. This can be understood as follows: With increasing f, the total mass of the star polymer increases and therefore the internal dynamics lasts longer time and hence there is a delayed crossover to superdiffusive behavior. The logarithmic crossover times for various star polymers with $n = 100$ and varying f for δ-correlated flow are listed in Table I. As τ_p is the same for star polymers with varying f (with fixed n), all these flows will represent the same Wi [see Eq. (13)]. The black dotted lines in the plot are the pure drift contribution from random

TABLE I. Logarithmic crossover times for star polymers with $n = 100$ and varying f and N for δ-correlated flow.

Functionality f	Total No. of beads N	Logarithmic crossover time $\log_{10}(t_c^*)$
2	201	4.02
3	301	4.26
6	601	4.62
12	1201	4.93

flow that matches asymptotically the ASD at longer times to further emphasize the intermediate stretching regime.

The scaling law obtained using fitting data from Eq. (43) for the star polymer shows two asymptotic regimes. For the intermediate-time regime, the scaling law relates the behavior of the star and linear polymer through

$$\frac{\overline{\langle Y^2_{\text{c.m.}}\rangle}_{\text{star}}}{\overline{\langle Y^2_{\text{c.m.}}\rangle}_{\text{linear}}} = \left(\frac{3(f-2)}{f^2}\right)^3, \tag{44}$$

while for the long-time regime (drift regime)

$$\frac{\overline{\langle Y^2_{\text{c.m.}}\rangle}_{\text{star}}}{\overline{\langle Y^2_{\text{c.m.}}\rangle}_{\text{linear}}} = \frac{3(f-2)}{f^2}\left(\frac{f}{2}\right)^{0.3}. \tag{45}$$

We can easily determine the crossover time of the star polymer if we know the same for the linear polymer as

$$\frac{(\tau_c)_{\text{star}}}{(\tau_c)_{\text{linear}}} = \frac{f}{2}. \tag{46}$$

To understand the influence of changing flow strength, we have plotted in Fig. 4 the scaled ASD vs scaled time for varying flow strength. Under the limit of negligible strength of external flow ($W \to 0$), the ASD reduces to the conventional diffusive motion, viz., Brownian diffusion (see the black line in the figure), i.e., linearly dependent on time. In the intermediate-time regime, as the flow strength increases, it results in an increase in the subdiffusive behavior due to the internal dynamics of the polymer. In the long-time regime, on

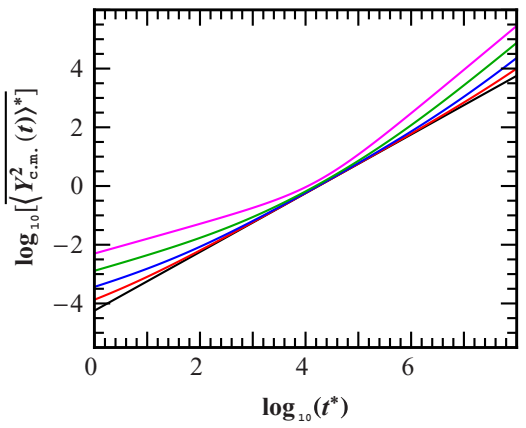

FIG. 4. (Color online) Influence of varying flow strength. Plotted on a logarithmic scale is $\overline{\langle Y^2_{\text{c.m.}}\rangle}^*$ vs t^* for the star polymer with $n = 100$ and $f = 3$ with varying W, i.e., $W = 0$, 2×10^{-19}, 8×10^{-19}, 32×10^{-19}, 128×10^{-19} a.u. (from bottom to top).

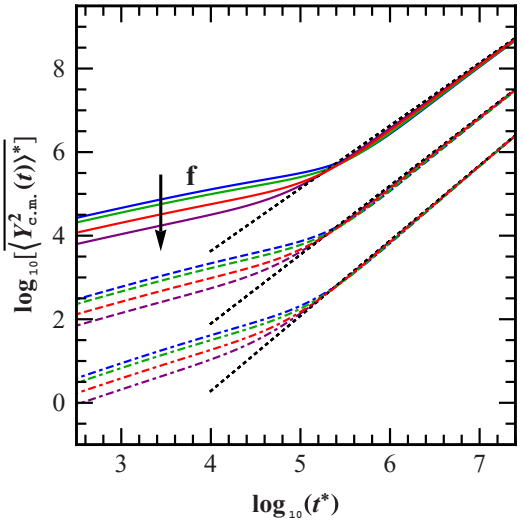

FIG. 5. (Color online) Dynamics of the center of mass of the star polymer under the influence of external random flow. Plotted on a logarithmic scale is $\overline{\langle Y^2_{\text{c.m.}}\rangle}^*$ vs t^* for star polymers with N fixed, i.e., $N = 1201$ and varying f, i.e., $f = 2$, 3, 6, and 12 (from top to bottom). We indicate the cases where $\alpha = 1$ (δ-correlated flow) by solid lines, $\alpha = 0.7$ (moderately correlated) by dashed lines, and $\alpha = 0.4$ (strongly correlated) by dot-dashed lines for $W = 5 \times 10^{-13}$ a.u. Black dotted lines represents the drift term due to random external flow.

increasing flow strength, the superdiffusive behavior increases due to the overall drift due to random flow of the polymer. So in the presence of the external flow, the diffusive behavior changes to subdiffusive in the intermediate-time regime and to superdiffusive in the long-time regime.

In Fig. 5 we display both the effect of the polymer topology and of the external random flow on the dynamics of the star polymer. The ASD is scaled by $\langle R_g^2\rangle$ for 1201 beads and is plotted against t^*. Further, $\overline{\langle Y^2_{\text{c.m.}}\rangle}^*$ is calculated according to Eq. (42) for various values of the flow parameter α. To understand the effect of the topology of the star polymer on its dynamics, we vary f while keeping N constant. We take $N = 1201$ and choose for the number of arms f the values 2, 3, 6, and 12. Here again two different regimes of motion are shown: the intermediate- (subdiffusive) and long-time (superdiffusive) regimes. The influence of the underlying topology on the dynamics is unraveled mainly in the intermediate-time regime. We observe that while keeping N fixed, the ASD increases as we decrease f of the star, while the long-time regime is only weakly dependent on the structure of the star polymer. Since N is constant, at very long time all the curves merge together, showing no influence of topology on the dynamics.

Another aspect that we study here is the effect of the external random flow on the dynamics. For this we study the same system, i.e., the star with $N = 1201$ and varying $f = 2$, 3, 6, and 12 for various values of the flow parameter α. We indicate the cases where $\alpha = 1$ (δ-correlated flow) by solid lines, $\alpha = 0.7$ (moderately correlated) by dashed lines, and $\alpha = 0.4$ (strongly correlated) by dot-dashed lines for $W = 5 \times 10^{-13}$ a.u. We observe that as we go from δ-correlated or weakly correlated to strongly correlated flow, there is a decrease in

the magnitude of the ASD, while the time dependence of the ASD increases as there is an increase in the slope in both time regimes, which is also evident from Eq. (42). The best power fits $\overline{\langle Y^2_{\text{c.m.}}\rangle} \propto t^{\nu}$ for $\alpha = 1$ give $\nu = 0.46 \pm 0.01$ in the intermediate-time regime and $\nu = 1.54 \pm 0.01$ in the long-time regime, for $\alpha = 0.7$ they give $\nu = 0.60 \pm 0.01$ in the intermediate-time regime and $\nu = 1.67 \pm .01$ in the long-time regime, and for $\alpha = 0.4$ they give $\nu = 0.71 \pm 0.01$ in the intermediate-time regime and $\nu = 1.82 \pm 0.01$ in the long-time regime. Also we observe that the crossover time from the subdiffusive to the superdiffusive regime remains almost constant for polymers with fixed N. For fixed molecular weight of the star polymers with increasing f, τ_p will decrease and hence the Wi of these flows decreases with functionality [see Eq. (13)]. The black dotted lines in the plot are the pure drift contributions of random flow that emphasize the intermediate stretching regime of the polymer.

B. Regular dendrimers

Dendrimers are defined as a class of macromolecules with highly branched treelike structures [80,81], which have vast biological applications [82,83]. As the number of generations of the dendrimer increases, it becomes more and more densely packed at the periphery and thus forms a closed membranelike structure. Thus, due to its unique architecture, the dendrimer has been gaining much attention in the field of energy transfer and has been used in artificial antenna systems for light harvesting [84,85]. A great deal of theoretical work has been done to study the dynamic and conformational properties of dendrimers [41–43,53–56,86–88]. Topologically these structures start at a central core from which f arms emerge. At each new generation g, the ends of the arms get $f - 1$ new arms attached to them (see Fig. 2). The structure ends at the G generation and the central core bead is considered to be the zeroth generation. For $f = 3$ the dendrimer consists of $N = 3(2^G - 1) + 1$ beads and the number of bonds is $N = 3(2^G - 1)$.

We display in Fig. 6 the long-time dependence of the ASD of the center of mass of dendrimers under external flow. Here again the scaled ASD (with an $\langle R_g^2\rangle$ of 22 beads) is plotted against dimensionless time t^* on a double-logarithmic scale for various generations $G = 3$, 5, and 7 using Eq. (42). From Fig. 6 we again observe two anomalous power-law regimes. We observe that the intermediate-time regime follows a subdiffusive power law, i.e., $\overline{\langle Y^2_{\text{c.m.}}\rangle} \propto t^{\nu}$, where $\nu < 1$, following which there is a crossover to the long-time regime showing superdiffusive dynamics with the exponent $\nu > 1$. Whereas the subdiffusive regime shows the intramolecular contributions to the ASD, the superdiffusive behavior indicates the diffusion of the polymer as a whole. Now the general trend of the ASD that is observed is that, in both the intermediate- and the long-time regime, as we increase the number of generations of the dendrimer, there is an increase in the magnitude of the ASD. This can be explained as follows: As the number of generations increases, there is an exponential increase in the total mass of the dendrimer that leads to greater stretching and also a greater overall diffusion of the polymer that is reflected in the intermediate- and long-time regimes, respectively. We observe that the maximum stretching of the dendrimer with

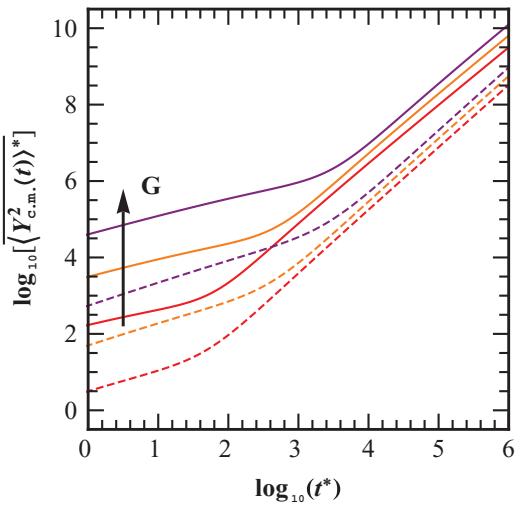

FIG. 6. (Color online) Dynamics of the regular dendrimer ($f = 3$) under the influence of external MdM flow. Plotted is $\overline{\langle Y^2_{\text{c.m.}}\rangle}^*$ vs dimensionless time t^* on a double-logarithmic scale for various generations $G = 3$, 5, and 7 (from bottom to top). We indicate the cases where $\alpha = 1$ (δ-correlated flow) by solid lines and $\alpha = 0.75$ (moderately correlated flow) by dashed lines for $W = 5 \times 10^{-11}$ a.u.

$G = 7$ is approximately four times greater than that of the linear polymer. Therefore, the higher-generation dendrimer moves faster than the lower-generation dendrimer due to random flow. A similar result was observed for the Rouse chain in Refs. [16,17], where it was shown that the ASD of the larger chain is greater compared to the ASD of the smaller chain.

The next important point that we observe in Fig. 6 is the delay in the crossover time t_c^* from subdiffusive to superdiffusive behavior as the generation of the dendrimer increases. The physical interpretation of this is that in the higher-generation dendrimer the internal dynamics is prolonged and hence delays the overall diffusion. This point is illustrated through Table II, which provides the logarithmic crossover times for various generations of dendrimers.

In Fig. 6 we also try to understand the effect of external flow by varying the value of α, where the solid lines indicate the case of weakly correlated or δ-correlated flow ($\alpha = 1$) and the dashed lines indicate moderately correlated flow ($\alpha = 0.75$). We observe that as we decrease the value of α, the magnitude of the ASD decreases. The power-law time dependence of the ASD increases with a decrease in α, which is reflected in the local slopes (in both time regimes of the logarithmic plots). The time dependence of the ASD is independent of the total mass and the topology of the polymer, while it varies with α

TABLE II. Logarithmic crossover times for various generations of dendrimers for δ-correlated flow.

Generation G	Total No. of beads N	Logarithmic crossover time $\log_{10}(t_c^*)$
3	22	1.80
5	94	2.72
7	382	3.51

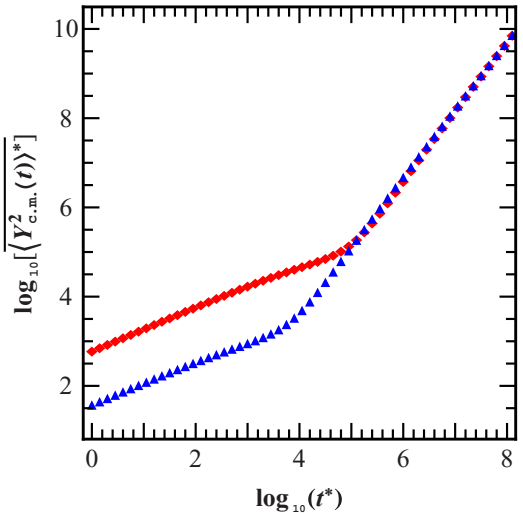

FIG. 7. (Color online) Comparison of the dynamics of the star and dendrimer with the same total number of beads $N = 766$ and functionality $f = 3$. Plot of $\overline{\langle Y^2_{\text{c.m.}}\rangle}^* = \overline{\langle Y^2_{\text{c.m.}}\rangle}/\langle R_g^2\rangle$ (R_g of 766 beads) vs t^* on a double-logarithmic scale with $\alpha = 1$ and $W = 5 \times 10^{-13}$ cm^3/s^2. Here red squares and blue triangles represent the curves for the star and dendrimer, respectively.

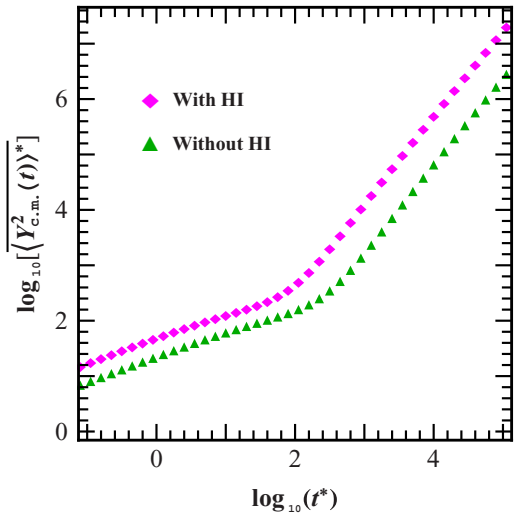

FIG. 8. (Color online) Comparison of the dynamics of the star with (magenta squares) and without (green triangles) HIs with $n = 3$ and $f = 4$. Plot of $\overline{\langle Y^2_{\text{c.m.}}\rangle}^*$ (scaled $\overline{\langle Y^2_{\text{c.m.}}\rangle}$ with $\langle R_g^2\rangle$ of the star polymer) vs t^* on a double-logarithmic scale with $\alpha = 1$ and $W = 5 \times 10^{-11}$ cm^3/s^2.

[see Eqs. (41) and (42)]. So for a particular exponential value of the flow, the intermediate- and long-time slopes remain the same for various generations of dendrimers. The best power fits $\overline{\langle Y^2_{\text{c.m.}}\rangle} \propto t^{\nu}$ for δ-correlated flow ($\alpha = 1$) give $\nu = 0.46 \pm 0.01$ in the intermediate-time regime and $\nu = 1.54 \pm 0.01$ in the long-time regime and for moderately correlated flow ($\alpha = 0.75$) they give $\nu = 0.58 \pm 0.01$ in intermediate-time regime and $\nu = 1.64 \pm 0.01$ in the long-time regime.

Finally, we compare the dynamics of the star and dendrimer with the same N and f, i.e., $N = 766$ and $f = 3$, under the external MdM flow with $\alpha = 1$ and $W = 5 \times 10^{-13}$ cm^3/s^2 (see Fig. 7). Here red squares indicate the curve for the star while blue triangles are for the dendrimer. In this plot we observe that the influence of the topology of the polymer is visible in the intermediate-time regime where the magnitude of the ASD of the star is greater than the ASD of the dendrimer. The long-time regime shows a weak dependence on the underlying topology of the polymer and both curves merge at a very long time. Also, it is shown that the crossover from the subdiffusive regime to the superdiffusive regime occurs faster in the case of the dendrimer than that of the star polymer due to the smaller overall size of the dendrimer compared to the star with the same total mass.

C. Contribution of HIs

The previous sections were focused on the understanding of the polymer dynamics in the absence of HIs. The purpose of this section is to give a brief idea of what the effect of the inclusion of HIs is on the dynamics of the branched polymer in the external random flow. A detailed mathematical formalism and analysis are beyond the scope of the present paper. As we know, the role of HIs in understanding the dynamical properties of polymer solutions has long been acknowledged. Zimm [89] extended the Rouse theory in order to take into account the HI effects using the preaveraged approximation. He obtained the theory of the relaxation behavior of long polymer chains in the absence of excluded-volume effects. Later the Zimm theory was extended to study in detail the intrinsic viscosity and the relaxation modes of branched polymers such as stars or dendrimers [90].

We use similar methodology to generalize our results with the inclusion of HIs using a preaverage approximation. We display in Fig. 8 the effect of inclusion of HIs on the ASD dynamics of the star polymer on a double logarithmic scale with $n = 3$ and $f = 4$. Here the Zimm (with HIs) and the Rouse (without HIs) cases are shown in magenta squares and green triangles, respectively. With the inclusion of HIs, the results suggest that while no qualitative change is seen, there is only a quantitative change due to the presence of HIs in the system. There are two main points of observation. First, taking HIs into account results in an increase in magnitude of the ASD, which is as expected as now there is an additional contribution of HIs that leads to faster displacement of the polymer. Second, as the longest relaxation times that are given by the smallest nonvanishing eigenvalues are shorter in the Zimm case than in the Rouse case, the presence of the hydrodynamic interactions speeds up the stretch dynamics and thus the overall drift occurs faster, which is shown by the crossover time that is shorter for the Zimm case than for the Rouse case.

IV. CONCLUSION

In this work we have developed a formalism to investigate the dynamics of arbitrary, flexible branched polymers in the presence of random flows. The modeling of flexible branched polymers is done within the framework of the GGS, while the random flow is accounted for through the MdM approach. Our approach is more general compared to previous

works [16,17,91], which are applicable for the Rouse-type linear chain polymers. Here we obtained a generalized expression for the ASD of the center of mass of branched polymers with complex underlying geometries, where the averages are done over both the thermal noise and the random external flow. We have analyzed the ASD dynamics of stars and dendrimers with varying topology under the influence of external flow. Both star and dendrimer structures show two anomalous power-law regimes of motion, viz., intermediate- and long-time regimes. The dynamics in the intermediate-time regime is observed due to the stretching and drift of the polymer structure that causes subdiffusive behavior. The dynamics in the long-time regime follows superdiffusive behavior, which is due to the random flow induced over all diffusion of the stretched polymer. The influence of external flow on the ASD is characterized by the flow exponent α. With a decrease in the value of α, there is a decrease in the magnitude of the ASD while its temporal exponent increases in both regimes. In the case of star polymers (with fixed N), it was observed that in the intermediate-time regime, the magnitude of the ASD increases with a decrease in f, while in the long-time regime there is a weaker dependence on f. Star polymers with fixed arm length and varying functionality show enhanced ASD magnitude with an increase in functionality. Subdiffusive and superdiffusive behaviors are independent of functionality but depend on flow behavior. Also, with increasing f, there is a delay in the crossover time from subdiffusive to superdiffusive behavior. In the case of dendrimers, with an increase in generation G, the magnitude of the ASD increases. The nature of intermediate-time subdiffusive and long-time superdiffusive behaviors is preserved, while their crossover times increase with an increase in G. It is known in the case of nonrandom flows that the smaller polymers move faster compared to the larger polymers [17,92]. In our analysis, we showed that the star and dendrimer with a greater total number of beads moves faster in random layered flow. This conclusion is similar to the one obtained for a linear Rouse chain in Refs. [16,17].

Finally, the dynamics of the star and dendrimer with N fixed are compared. The influence of the underlying topology on the dynamics is observed mainly in the intermediate-time regime where the ASD of the star is greater than that of the dendrimer. The long-time regime shows a weaker dependence on the polymer structure. Also the crossover time between these regimes for the star is greater than that of the dendrimer, i.e., the star polymer takes a longer time to diffuse as a whole due to its greater overall size as compared to the dendrimer of the same total mass.

ACKNOWLEDGMENTS

D.K. is thankful to CSIR for providing funding through a Senior Research Fellowship (SRF). R.K. is grateful to the University of Delhi for support through R&D and DST SERB grants.

APPENDIX: LONG-TIME APPROXIMATION

For the long-time limit, i.e., $|t' - t''| > \tau_R$, Eq. (41) can be simplified by dropping the exponential term and substituting $t' = 0$ as

$$\langle [X_m(0) - X_n(t'')]^2 \rangle \approx \frac{2k_BT}{N\zeta} t'' + \frac{k_BT}{\sigma\zeta} \sum_{i\neq 1} \left[Q_{mi} Q_{im}^{-1}/\lambda_i + Q_{ni} Q_{in}^{-1}/\lambda_i \right]. \tag{A1}$$

Solving the double integral in Eq. (32) using Eq. (A1), we obtain

$$\begin{aligned}
\int_0^t dt' \int_0^{t'} dt'' \langle [X_m(0) - X_n(t'')]^2 \rangle^{-\alpha/2} &= \frac{1}{(4-\alpha)(2-\alpha)} \left(\frac{\zeta N}{2k_BT} \right)^2 \left\{ 4 \left(\frac{k_BT}{\sigma\zeta} \sum_{i\neq 1} C_i^{mn} + \frac{2k_BT}{N\zeta} t \right)^{2-\alpha/2} \right. \\
&\quad \left. - 4(4-\alpha) \left(\frac{k_BT}{\sigma\zeta} \sum_{i\neq 1} C_i^{mn} \right)^{1-\alpha/2} \left(\frac{k_BT}{N\zeta} \right) t - 4 \left(\frac{k_BT}{\sigma\zeta} \sum_{i\neq 1} C_i^{mn} \right)^{2-\alpha/2} \right\} \\
&= \frac{1}{(4-\alpha)(2-\alpha)} \left(\frac{\zeta N}{2k_BT} \right)^2 \left\{ 4 \left(\frac{2k_BT}{N\zeta} t \right)^{2-\alpha/2} \left[1 + \frac{(4-\alpha)}{4} \left(\frac{N\zeta}{k_BT} \right) \right. \right. \\
&\quad \left. \times \left(\frac{b^2}{3} \sum_{i\neq 1} C_i^{mn} \right) t \right] - 2(4-\alpha) \left(\frac{b^2}{3} \sum_{i\neq 1} C_i^{mn} \right)^{1-\alpha/2} \left(\frac{2k_BT}{N\zeta} t \right) \\
&\quad \left. - 4 \left(\frac{b^2}{3} \sum_{i\neq 1} C_i^{mn} \right)^{2-\alpha/2} \right\},
\end{aligned} \tag{A2}$$

where $C_i^{mn} = Q_{mi} Q_{im}^{-1}/\lambda_i + Q_{ni} Q_{in}^{-1}/\lambda_i$. Finally, we substitute Eq. (A2) in Eq. (32) to get the final ASD expression for the long-range correlation given by Eq. (42).

[1] T. T. Perkins, D. E. Smith, and S. Chu, Science **276**, 2016 (1997).
[2] D. E. Smith and S. Chu, Science **281**, 1335 (1998).
[3] D. E. Smith, H. P. Babcock, and S. Chu, Science **283**, 1724 (1999).
[4] P. LeDuc, C. Haber, G. Boa, and D. Wirtz, Nature (London) **399**, 564 (1999).
[5] C. M. Schroeder, H. P. Babcock, E. S. G. Shaqfeh, and S. Chu, Science **301**, 1515 (2003).
[6] S. R. Quake, H. Babcock, and S. Chu, Nature (London) **388**, 151 (1997).
[7] R. G. Larson, J. Rheol. **49**, 1 (2005).
[8] J. L. Lumley, Annu. Rev. Fluid. Mech. **1**, 367 (1969).
[9] J. L. Lumley, Symp. Math. **9**, 315 (1972).
[10] M. D. Graham, Annu. Rev. Fluid Mech. **43**, 273 (2011).
[11] S. Gerashchenko and V. Steinberg, Phys. Rev. Lett. **96**, 038304 (2006).
[12] H. P. Babcock, R. E. Teixeira, J. S. Hur, E. S. G. Shaqfeh, and S. Chu, Macromolecules **36**, 4544 (2003).
[13] R. Rzehak, W. Kromen, T. Kawakatsu, and W. Zimmermann, Eur. Phys. J. E **2**, 3 (2000).
[14] F. Brochard Wyart, Europhys. Lett. **23**, 105 (1993).
[15] C.-C. Huang, R. G. Winkler, G. Sutmann, and G. Gompper, Macromolecules **43**, 10107 (2010).
[16] G. Oshanin and A. Blumen, Phys. Rev. E **49**, 4185 (1994).
[17] G. Oshanin and A. Blumen, Macromol. Theory Simul. **4**, 87 (1995).
[18] A. Groisman and V. Steinberg, Phys. Rev. Lett. **86**, 934 (2001).
[19] S. Gerashchenko, C. Chevallard, and V. Steinberg, Europhys. Lett. **71**, 221 (2005).
[20] M. Martins Afonso and D. Vincenzi, J. Fluid Mech. **540**, 99 (2005).
[21] A. Celani, S. Musacchio, and D. Vincenzi, J. Stat. Phys. **118**, 531 (2005).
[22] A. Groisman and V. Steinberg, Nature (London) **405**, 53 (2000).
[23] A. Groisman and V. Steinberg, New J. Phys. **6**, 29 (2004).
[24] Y. Liu and V. Steinberg, Europhys. Lett. **90**, 44005 (2010).
[25] M. Chertkov, I. Kolokolov, V. Lebedev, and K. Turitsyn, J. Fluid Mech. **531**, 251 (2005).
[26] J. Davoudi and J. Schumacher, Phys. Fluids **18**, 025103 (2006).
[27] K. Turitsyn, JETP **105**, 655 (2007).
[28] Y. Liu and V. Steinberg, Macromol. Symp. **337**, 34 (2014).
[29] E. Balkovsky, A. Fouxon, and V. Lebedev, Phys. Rev. Lett. **84**, 4765 (2000).
[30] M. Chertkov, Phys. Rev. Lett. **84**, 4761 (2000).
[31] A. Celani, A. Puliafito, and D. Vincenzi, Phys. Rev. Lett. **97**, 118301 (2006).
[32] A. A. Gurtovenko and A. Blumen, Adv. Polym. Sci. **182**, 171 (2005).
[33] M. Ripoll, R. G. Winkler, and G. Gompper, Phys. Rev. Lett. **96**, 188302 (2006).
[34] S. V. Lyulin, A. A. Darinskii, A. V. Lyulin, and M. A. J. Michels, Macromolecules **37**, 4676 (2004).
[35] P. E. Rouse, J. Chem. Phys. **21**, 1272 (1953).
[36] M. Doi and S. F. Edwards, *The Theory of Polymer Dynamics* (Clarendon, Oxford, 1986).
[37] J. U. Sommer and A. Blumen, J. Phys. A **28**, 6669 (1995).
[38] H. Schiessel, Phys. Rev. E **57**, 5775 (1998).
[39] C. Friedrich, H. Schiessel, and A. Blumen, in *Advances in the Flow and Rheology of Non-Newtonian Fluids*, edited by D. A. Siginer, D. DeKee, and R. P. Chhabra (Elsevier, Amsterdam, 1999), p. 429.
[40] H. Schiessel, C. Friedrich, and A. Blumen, in *Applications of Fractional Calculus in Physics*, edited by R. Hilfer (World Scientific, Singapore, 1999).
[41] R. Kant, P. Biswas, and A. Blumen, Macromol. Theory Simul. **9**, 608 (2000).
[42] P. Biswas, R. Kant, and A. Blumen, Macromol. Theory Simul. **9**, 56 (2000).
[43] P. Biswas, R. Kant, and A. Blumen, J. Chem. Phys. **114**, 2430 (2001).
[44] C. Satmarel, C. von Ferber, and A. Blumen, J. Chem. Phys. **124**, 174905 (2006).
[45] C. Satmarel, C. von Ferber, and A. Blumen, J. Chem. Phys. **123**, 034907 (2005).
[46] A. Blumen and A. Jurjiu, J. Chem. Phys. **116**, 2636 (2002).
[47] A. Jurjiu, T. Koslowski, and A. Blumen, J. Chem. Phys. **118**, 2398 (2003).
[48] A. Blumen, C. von Ferber, A. Jurjiu, and T. Koslowski, Macromolecules **37**, 638 (2004).
[49] A. Jurjiu, T. Koslowski, C. von Ferber, and A. Blumen, Chem. Phys. **294**, 187 (2003).
[50] A. A. Gurtovenko and A. Blumen, J. Chem. Phys. **115**, 4924 (2001).
[51] A. Blumen, A. A. Gurtovenko, and S. Jespersen, J. Non-Cryst. Solids **305**, 71 (2002).
[52] J. Roovers and B. Comanita, Adv. Polym. Sci. **142**, 179 (1999).
[53] F. Ganazzoli, R. LaFerla, and G. Raffaini, Macromolecules **34**, 4222 (2001).
[54] Z. Y. Chen and C. Cai, Macromolecules **32**, 5423 (1999).
[55] C. Cai and Z. Y. Chen Macromolecules **30**, 5104 (1997).
[56] R. LaFerla, J. Chem. Phys. **106**, 688 (1997).
[57] M. Bixon and R. Zwanzig, J. Chem. Phys. **68**, 1896 (1978).
[58] M. Dolgushev and A. Blumen, J. Chem. Phys. **138**, 204902 (2013).
[59] M. Dolgushev and A. Blumen, J. Chem. Phys. **131**, 044905 (2009).
[60] A. Kumar and P. Biswas, Macromolecules **43**, 7378 (2010).
[61] A. Kumar and P. Biswas, J. Chem. Phys. **137**, 124903 (2012).
[62] S. P. Singh, A. Chatterji, G. Gompper, and R. G. Winkler, Macromolecules **46**, 8026 (2013).
[63] A. Nikoubashman and C. N. Likos, Macromolecules **43**, 1610 (2010).
[64] G. Matheron and G. de Marsily, Water Resour. Res. **16**(5), 901 (1980).
[65] B. E. Eichinger and J. E. Martin, J. Chem. Phys. **69**, 4595 (1978).
[66] A. Kloczkowski, J. E. Mark, and H. L. Frisch, Macromolecules **23**, 3481 (1990).
[67] A. Peterlin, J. Polym. Sci., Part B: Polym. Lett. **4**, 287 (1966).
[68] A. Papoulis, *Probability, Random Variables, and Stochastic Processes*, 3rd ed. (McGraw-Hill, New York, 1991).
[69] B. Gaveau and L. S. Schulman, J. Stat. Phys. **66**, 375 (1992).
[70] G. S. Grest, L. J. Fetters, J. S. Huang, and D. Richter, Adv. Chem. Phys. **XCIV**, 67 (1996).
[71] M. Daoud and J. P. Cotton, J. Phys. (France) **43**, 531 (1982).
[72] J. Roovers, L.-L. Zhou, P. M. Toporowski, M. van der Zwan, H. Iatrou, and N. Hadjichristidis, Macromolecules **26**, 4324 (1993).
[73] L. J. Fetters, A. D. Kiss, D. S. Pearson, G. F. Quack, and F. J. Vitus, Macromolecules **26**, 647 (1993).

[74] B. J. Bauer, L. J. Fetters, W. W. Graessley, N. Hadjichristidis, and G. F. Quack, Macromolecules **22**, 2337 (1989).
[75] K. Huber, S. Bantle, W. Burchard, and L. Fetters, Macromolecules **19**, 1404 (1986).
[76] L. Willner, O. Jucknischke, D. Richter, J. Roovers, L.-L. Zhou, P. M. Toporowski, L. J. Fetters, J. S. Huang, M. Y. Lin, and N. Hadjichristidis, Macromolecules **27**, 3821 (1994).
[77] D. W. Dozier, J. S. Huang, and L. J. Fetters, Macromolecules **24**, 2810 (1991).
[78] S. S. Stivala, B. A. Khorramian, and A. Patel, Polymer **27**, 517 (1986).
[79] S. Jin, K. S. Jin, J. Yoon, K. Heo, J. Kim, K.-W. Kim, M. Ree, T. Higashihara, T. Watanabe, and A. Hirao, Macromol. Res. **16**, 686 (2008).
[80] J. M. J. Frechet, Science **263**, 1710 (1994).
[81] G. R. NewKome, *Advances in Dendritic Macromolecules* (JAI, London, 1996).
[82] R. Esfand and D. A. Tomalia, Drug Discov. Today **6**, 427 (2001).
[83] K. Kono, T. Miyoshi, Y. Haba, E. Murakami, C. Kojima, and A. Harada, J. Am. Chem. Soc. **129**, 7222 (2007).
[84] A. Bar-Haim, J. Klafter, and R. Kopelman, J. Am. Chem. Soc. **119**, 6197 (1997).
[85] A. Nantalaksakul, D. R. Reddy, C. J. Bardeen, and S. Thayumanavan, Photosynth. Res. **87**, 133 (2006).
[86] P. Biswas and B. J. Cherayil, J. Chem. Phys. **100**, 3201 (1994).
[87] F. Ganazzoli and R. LaFerla, J. Chem. Phys. **113**, 9288 (2000).
[88] A. A. Gurtovenko, D. A. Markelov, Y. Y. Gotlib, and A. Blumen, J. Chem. Phys. **119**, 7579 (2003).
[89] B. H. Zimm, J. Chem. Phys. **24**, 269 (1956).
[90] B. H. Zimm and R. W. Kilb, J. Polym. Sci. **37**, 19 (1959).
[91] S. Jespersen, G. Oshanin, and A. Blumen, Phys. Rev. E **63**, 011801 (2000).
[92] G. Zumofen, J. Klafter, and A. Blumen, J. Stat. Phys. **65**, 991 (1991).